Atmospheric Pollution Research 11 (2020) 482–490

HOSTED BY

Contents lists available at ScienceDirect

Atmospheric Pollution Research

journal homepage: www.elsevier.com/locate/apr

Mitigating MODIS AOD non-random sampling error on surface $PM_{2.5}$ estimates by a combined use of Bayesian Maximum Entropy method and linear mixed-effects model

Disong Fu[a,f], Zijue Song[a,c], Xiaoling Zhang[c], Xiangao Xia[a,b,f,*], Jun Wang[d,**], Huizheng Che[e], Huangjian Wu[f,g,h], Xiao Tang[g], Jinqiang Zhang[a,b], Minzheng Duan[a,c,f]

[a] LAGEO, Institute of Atmospheric Physics, Chinese Academy of Sciences, Beijing, 100029, China
[b] Collaborative Innovation Center on Forecast and Evaluation of Meteorological Disasters, Nanjing University of Information Science & Technology, Nanjing, 210044, China
[c] Chengdu University of Information Technology, Chengdu, 610225, China
[d] Department of Chemical and Biochemical Engineering, Center for Global and Regional Environmental Studies, The University of Iowa, Iowa City, IA, 52241, USA
[e] Key Laboratory of Atmospheric Chemistry (LAC), Chinese Academy of Meteorological Sciences (CAMS), CMA, Beijing, 100081, China
[f] College of Earth and Planetary Sciences, University of Chinese Academy of Sciences, Beijing, 100049, China
[g] LAPC, Institute of Atmospheric Physics, Chinese Academy of Sciences, Beijing, 100029, China
[h] Guanghua School of Management, Peking University, Beijing, 100029, China

ARTICLE INFO

Keywords:
BME
LME
$PM_{2.5}$
North China plain
CARSNET
MODIS
AERONET

ABSTRACT

$PM_{2.5}$ estimates solely based on the Moderate Resolution Imaging Spectroradiometer (MODIS) AOD products may lead to a substantial bias because of non-random AOD sampling deficiency in cloudy conditions and swap-gap regions. Furthermore, this non-random sampling issue can be exacerbated in polluted regions where heavy aerosol loadings are likely misclassified into clouds. Here, to mitigate non-random sampling deficiency in MODIS AOD product for surface-level $PM_{2.5}$ estimates, we have combined Bayesian maximum entropy (BME) method with the Linear Mixed-Effects (LME) model, for the first time, to produce more spatiotemporally complete and precise AOD products and thereafter $PM_{2.5}$ estimates. This combined BME-LME approach was applied to MODIS and sunphotometer AOD products over the North China Plain. Relative to the standard MODIS AOD product, the integration of MODIS and sunphotometer AOD through BME showed increases in both spatiotemporal completeness (up to 96%) and the quality. The resultant monthly $PM_{2.5}$ estimates from the BME-LME had a bias of 3.5 μg m^{-3} and a root mean square error (RMSE) of 5.5 μg m^{-3}, showing substantial improvement over $PM_{2.5}$ estimations from original MODIS AOD product (a bias of 84.1 and a RMSE of 112.1 μg m^{-3}). Merging sunphotomter and satellite AOD observations with BME-LME is a prospective method to simultaneously improve AOD and $PM_{2.5}$ estimates.

1. Introduction

Knowledge of spatiotemporal distribution of fine particulate matter with aerodynamic diameter of 2.5 μm or less ($PM_{2.5}$) is highly needed since $PM_{2.5}$ particles can enter the lungs, cause respiratory diseases, increase risk of cardiovascular and even lung cancer (Hoek et al., 2013; Pope and Dockery, 2006; Pope III, 2002; Pui et al., 2014). Establishment of ground monitoring network is the ideal way to accurately measure ground-level $PM_{2.5}$ concentration, which is exactly why thousands of ground sites have been deployed in the United States and Western Europe (Li et al., 2015; Van Donkelaar et al., 2015). However, sparse geographic coverage of the network is not dense enough for monitoring $PM_{2.5}$ at spatial scales of a few kilometers (Gupta et al., 2016). and maintaining such networks are very costly. In addition, most developing nations have few or no surface $PM_{2.5}$ measurements, therefore, alternative methods are highly required to monitor $PM_{2.5}$.

It has been proved that satellite-based aerosol optical depth (AOD), the column-integrated aerosol extinction, is a good surrogate for $PM_{2.5}$ (Wang and Christopher, 2003). Since then, ground-level $PM_{2.5}$ concentrations have been estimated from many satellite sensors, for

Peer review under responsibility of Turkish National Committee for Air Pollution Research and Control.
* Corresponding author. LAGEO, Institute of Atmospheric Physics, Chinese Academy of Sciences, Beijing, 100029, China.
** Corresponding author.
E-mail addresses: xxa@mail.iap.ac.cn (X. Xia), jun-wang-1@uiowa.edu (J. Wang).

https://doi.org/10.1016/j.apr.2019.11.020
Received 20 August 2019; Received in revised form 22 November 2019; Accepted 22 November 2019
Available online 27 November 2019

example, Moderate Resolution Imaging Spectroradiometer (MODIS), Multi-angle Imaging SpectroRadiometer (MISR), Polarization and Directionality of the Earth's Reflectances (POLDER) onboard PARASOL, and Visible Infrared Imaging Radiometer Suite (VIIRS). Numerous methods have been adopted to address the relationship between AOD and $PM_{2.5}$ (AOD-$PM_{2.5}$) varying from conventional linear regression to advanced machine learning algorithms (Chudnovsky et al., 2013; Liu et al., 2005; Van Donkelaar et al., 2016; Wu et al., 2016). Much effort has been paid to obtain better AOD-$PM_{2.5}$ relationships for which the availability of AOD from space is one of fundamental requirements. Unfortunately, non-random missing values in AOD retrievals often occur due to cloud cover, high surface reflectance (Xiao et al., 2017) or even misclassification of heavy pollution to clouds (Fu et al., 2018; Song et al., 2018), let alone to mention the inherent limitations of these satellites in spatial and temporal coverage (Geng et al., 2015; Strickland et al., 2016; Zhan et al., 2017). This very likely leads to a substantial bias of $PM_{2.5}$ estimation since the difference between $PM_{2.5}$ concentrations in the presence and absence of satellite AOD retrievals may be substantially large, for example, the difference in monthly $PM_{2.5}$ concentration could exceed 20 μg m^{-3} at some heavily polluted sites in North China (Song et al., 2019).

A couple of methods have been implemented to fill AOD gaps. A combination MODIS and MISR AOD products has been approved to improve coverage, especially in western China where AOD is not available from the operational MODIS dark target algorithm (Ma et al., 2014). Certainly, cloud contamination and misclassification of heavy aerosol loading cannot be resolved by this method. The cloud screening criteria of the MODIS algorithm was relaxed to increase AOD coverage during a biomass burning episode in Moscow (Van Donkelaar et al., 2011), which was mainly adopted by case studies. Fu et al. (2018) merged Aerosol Robotic Network (AERONET) and MODIS AOD products to increase AOD sampling rate by 59% in winter when the MODIS aerosol algorithm may not provide AOD product in many cases. This method is subjected to sparse coverage of AERONET stations. Xiao et al. (2017) combined satellite AOD with chemical transport model (CTM) simulations to fill AOD gaps. This method is subjected to the CTM uncertainty and its relatively coarse spatial resolution, although the spatial resolution of some CTM simulations can be as high as 5 km (or less with high computation demand) in regional scale. Statistical methods are developed to fill satellite AOD gaps, for example, the kriging interpolation method, $PM_{2.5}$ based iterative imputation, multiple imputation and machine learning methods have been shown great potential in filling AOD gaps (Lv et al., 2017; Xiao et al., 2017; Zhang et al., 2018). These methods need many extra inputs that may be unavailable in many cases, in addition, AOD uncertainties have not be fully considered.

Given the fact that the Bayesian Maximum Entropy (BME) developed by Christakos (1990a, 1990b) can fully take advantage of the high-order space/time moments of AOD fields as wells as explicitly account for the uncertainties of the measurements, it has potential to tackle missing AODs. The BME has been widely applied in spatiotemporal estimation (He and Christakos, 2018; Shi et al., 2015; Zhang et al., 2018), in particular, showing encouraging performance in filling missing AODs from multiple-sensor AOD retrievals (Tang et al., 2016).

North China Plain (NCP: 34.4–42.6° N; 113.5–122.7° E) is one of heavily populated plain in the world, which is often attacked by widespread heavy air pollution events. Much progress has been in ground remote sensing AODs by the establishment of sun photometers as a part of the Aerosol Robotic Network (AERONET) and China Aerosol Remote Sensing Network (CARSNET) (Che et al., 2014). The objective of this study is to enhance AOD sampling rate by using the BME method and study how such enhancement may improve $PM_{2.5}$ estimation. The study differs from previous studies in following aspects. First, uncertainties associated with satellite AOD are carefully evaluated and accounted for. Second, both AERONET and CARSNET AOD products are synergized to improve AOD filling. Third, BME-based filling AODs are evaluated against independent sunphotometer measurements. Fourth, potential errors of monthly $PM_{2.5}$ estimation from AOD are detailed evaluated. The paper is organized as follows. Section 2 introduces AOD and $PM_{2.5}$ data. The BME is described in Section 3. The results of BME-based AOD and corresponding $PM_{2.5}$ concentration prediction are illustrated in Section 4.

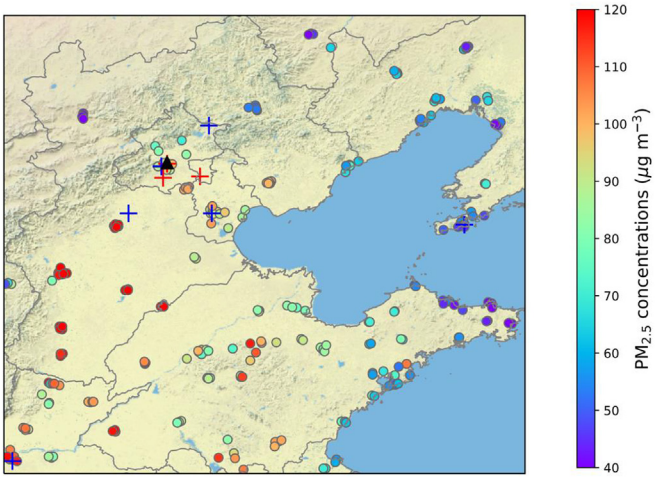

Fig. 1. Spatial distribution $PM_{2.5}$ stations and their annual average concentration (μg m^{-3}) in North China Plain. The plus markers are the AERONET/CARSNET sites (green for AEORNET and blue for CARSNET). AERONET RADI site is specially marked as triangle point.

2. Materials and methods

2.1. AERONET and CARSNET

Ground-based AOD measurements from Sun-photometers (Cimel Electronique, CE-318) were collected at 9 stations as a part of CARSNET or AERONET in NCP (Fig. 1). Stations are installed at diverse landscapes, for example, in mega-cities (Beijing and Tianjin), suburban region (Xianghe) and background area (for example, Shangdianzi, a station at the top of hills). CIMEL Sun-photometer makes direct spectral solar radiation measurements in a 1.2° field of view angle every nominal 15 min (Holben et al., 1998). Direct solar spectral radiation at wavelengths from 0.34 μm to 1.02 μm is used to derive spectral AOD with accuracy of 0.01–0.02 (Che et al., 2014; Eck et al., 1999). AOD at 0.55 μm is interpolated from AOD at 0.44, 0.67 and 0.87 μm. The latest Version 3 cloud-screened and quality assured AOD data (Level 2.0) are used for calculating daily mean AOD. These daily AOD data are taken as hard data in the BME method. To validate filling AOD products, we choose the Level 1.5 AOD measurements at Beijing RADI site (not used in the BME method) as the independent dataset in the validation.

2.2. MODIS AOD

Even though the MODIS sensors aboard Terra and Aqua have operated for more than a decade, the algorithms are still being updated (Hsu et al., 2013; Levy et al., 2013). The latest Collection 6.1 was completed and released in March 2018 that was used in this study. The MODIS Adaptive Processing System (MODAPS) uses two mainstream algorithms, dark target (DT) and deep blue (DB), for the retrievals. In brief, DT algorithm parameterized the ratio of the surface reflectance at 0.47 and 0.65 μm to that at 2.13 as a function of view angle and normalized vegetation index (Levy et al., 2013). The DB method expands MODIS AOD coverage to bright arid surfaces by using MODIS reflectance measurement at 0.412 μm, where surface reflectance is relatively dark (Hsu et al., 2013).

Compared to C6, a revised surface characterization when the urban

percentage is greater than 20% is adopted in the C6.1 DT algorithm. This can correct AOD biases over urban areas and increase AOD retrievals falling within expected error by 20% (Gupta et al., 2016). Regarding the DB algorithm, several principal improvements include artifact reduction in heterogeneous terrain and improved surface modeling in elevated terrain. Since heavy smoke events could sometimes be identified as cloud in the C6 DB algorithm, internal smoke detection masks have been improved to minimize false cloud contamination (Eck et al., 2018). Although the 3 km AOD product (only the DT algorithm) was available in 2016 that is widely used in the estimation of $PM_{2.5}$ (Gupta et al., 2018), here MODIS 10 km AOD merged DT and DB product is used because of very few 3 km AOD retrievals in the winter season in NCP (4%).

The MODIS AOD data are gridded into 10 km by 10 km by using the nearest-neighbor interpolation method. Given the fact that AOD shows a distinct diurnal variation in NCP (Qu et al., 2016; Song et al., 2018; Xia et al., 2006) and daily AOD sampling rate can be improved by a combination of Terra and Aqua AOD (Ma et al., 2014), we combine these two datasets by following procedures to obtain a more completed and accurate daily AOD. First, the linear regression analysis is used to build the relationship between Terra and Aqua AODs for each grid if both are available. Second, missing Terra (Aqua) AOD is filled by using the linear-fit equation (1) with Aqua (Terra) AOD if available.

$$AOD_{Terra-fit,i} = a_i * AOD_{Aqua,i} + b_i$$

$$AOD_{Aqua-fit,i} = (AOD_{Terra,i} - b_i)/a_i \quad (1)$$

where i represents the grid, a_i and b_i are slope and intercept from linear regression for the grid. Third, the combined AOD are obtained as follows:

$$AOD_{combine} = \begin{cases} (AOD_{Aqua} + AOD_{Terra})/2 & (both\ \ avaialbe) \\ (AOD_{Aqua} + AOD_{Terra-fit})/2 & (only\ Aqua\ avaialbe) \\ (AOD_{Aqua-fit} + AOD_{Terra})/2 & (only\ Terra\ avaiable) \\ NA & (both\ absent) \end{cases} \quad (2)$$

2.3. $PM_{2.5}$ data

Hourly $PM_{2.5}$ concentrations from September 2014 to February 2015 at 264 monitors (Fig. 1) are obtained from the website of the China Environmental Monitoring Center (CEMC) (http://106.37.208.233:20035/). Detailed data quality assurance was applied to discriminate four types of outliers (Wu et al., 2018).

(1) Spatiotemporal inconsistent outliers: values greatly deviated from other values observed at the adjacent time (one month) or in neighboring areas (25 km); (2) Low variance outliers: data points having a very low temporal variance compared with adjacent sites, likely as a result of the depletion of the filter tape; (3) Periodic outliers: those abnormal values occurring every 24 h caused by the regular calibration for the instruments; (4) outliers characterized by PM_{10} smaller than $PM_{2.5}$.

Based on these quality-controlled hourly $PM_{2.5}$ data, we calculate daily average $PM_{2.5}$ concentrations if there are 20 hourly measurements each day.

2.4. The linear mixed-effects model

There are many methods to estimate $PM_{2.5}$ from AOD. Here we use linear mixed-effects model (LME) to estimate $PM_{2.5}$ concentrations from AOD products as a result of its simplicity and robustness (LME) (Lee et al., 2011).

$$PM_{i,j} = (\alpha + u_j) + (\beta + v_j)AOD_{i,j} + s_i + \varepsilon_{i,j} \quad (3)$$

$$(u_j v_j \sim N[(00), \sum])$$

where $PM_{i,j}$ represents $PM_{2.5}$ value at site i on day j; α and β are fixed intercept and slope; u_j and v_j are the random intercept and slope. $s_i \sim N(0\sigma_s^2)$ and $\varepsilon_{i,j} \sim N(0\sigma^2)$ represent the random intercept of site i and the error term at site i on day j, respectively. σ_s^2 and σ^2 denote the variances for s_i and $\varepsilon_{i,j}$. Σ is the variance-covariance matrix for the day-specific random effects.

The LME model, with a nested form, establishes the day-specific $PM_{2.5}$-AOD relationships that are based on daily AOD and $PM_{2.5}$ at 264 stations in NCP. Compared with more complicated models, the LME model can predict $PM_{2.5}$ from a single independent variable AOD with comparable quality to other methods. The ten-fold cross-validation (CV) approach was used to assess the performance of the method. For this cross-validation, we randomly divided the data pairs into 10 equal-size groups. At each of 10 iterations, 9 groups of data were used to build a day-specific LME model, and the remaining group was used to test its performance.

2.5. The BME method

The BME is a nonlinear interpolation method and provides a rigorous approach for integrating various physical knowledge: general knowledge (G-KB, such as statistical moments of any order, physical laws, scientific theories, empirical relationships) and site-specific knowledge (S-KB; including hard AOD data obtained from site measurements and soft data characterized by considerable degrees of uncertainty (Christakos and Serre, 2000; Yu et al., 2007). The nonlinear mean estimation $\overline{x_k}$ of AOD at time t of a grid cell can be estimated by AOD measurements from adjacent time or neighboring areas:

$$\overline{x_k} = \int x_k f(x_k|x_{obs})dx_k \quad (4)$$

$$x_{obs} = (x_{soft}, x_{hard})$$

where x_{obs} means the observed field consisting of soft data and hard data. $f(x_k|x_{obs})$ is the posterior probability density function (PDF) and can be calculated according to the Bayesian rule.

$$f(x_k|x_{obs}) = \frac{f(x_{obs}, x_k)}{f(x_{obs})} = \frac{f(x_{map})}{f(x_{obs})} \quad (5)$$

where $f(x_{obs})$ is the prior PDF of the x_{obs} data. Specifically, the hard data are mean CIMEL observation data and the soft data represent MODIS AOD. $f(x_{map}) = f(x_{obs}, x_k)$ is a joint PDF that is derived by maximizing the entropy under the constraint of the G-KB. A set of statistical moments can represent the G-KB stochastically according to equation (6). For example, the mean and covariance space/time moment are obtained from equation (6) if g_α is x_i and $(x_i - \overline{x_i})(x_j - \overline{x_j})$ (the bar denotes stochastic expectation).

$$\overline{g_\alpha(x_{map})} = \int dx_{map} \Big) g_\alpha(x_{map}) f(x_{map}) \quad (6)$$

$$H = -\int d(x_{map}) f(x_{map}) log f(x_{map}) \quad (7)$$

To maximize H in equation (7) subject to the physical constraints in Eq. (6), $G_\alpha[f(x_{map})] = \int dx_{map} g_\alpha(x_{map}) f(x_{map}) - \overline{g_\alpha(x_{map})}$ is set and Lagrange multiplier is introduced.

$$L[f(x_{map})] = H - \sum_{\alpha=0}^{N} \lambda_\alpha \cdot G_\alpha[f(x_{map})] \quad (8)$$

Setting the partial derivatives to zero and solving the system of equations with respect to the λ_α yields the maximum entropy solution for joint PDF $f(x_{map})$. Finally, the joint PDF is substituted in equations (5) and (4) to solve $\overline{x_k}$ (Christakos and Serre, 2000; Modis et al., 2013;

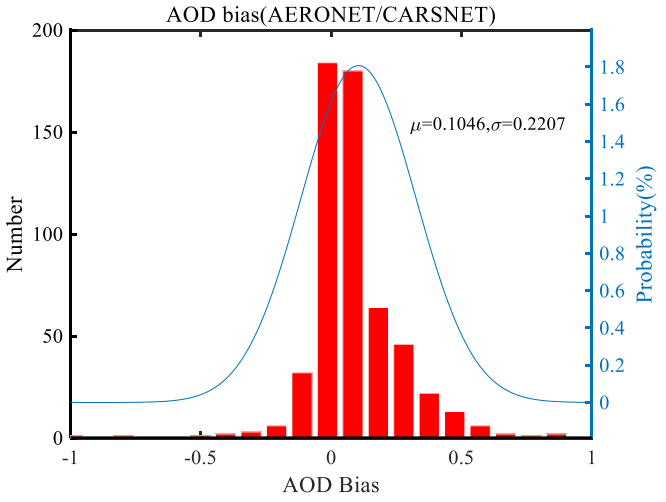

Fig. 2. Gaussian probability density function of ε.

Tang et al., 2016; Yu et al., 2007).

Daily mean AODs at AERONET and CARSNET stations are calculated and taken as the hard data for the BME algorithm. Soft data are assumed to be in the shape of probability functions and constructed by comparing the satellite and sun-photometer AODs. The uncertainty of soft data is calculated as follows.

$$AOD_{combine} = AOD_{sun-photometer} + \varepsilon \quad (9)$$

$$\varepsilon \sim N(\mu,\ \sigma^2)$$

Daily sun-photometer and MODIS AOD are collocated to estimate the difference (ε) and its PDF. ε is assumed to follow the normal distribution with mean (μ) and variance (σ^2) (Fig. 2). For pixels with satellite AODs are available, the Gaussian distribution probability soft data follows the normal distribution $N(AOD_{combine} - \mu,\ \sigma^2)$.

Mean and covariance of satellite AOD are served as $\overline{g_\alpha(x_{map})}$ in this study. To meet the assumption of second-order stationarity (constant mean and variance) throughout the spatiotemporal domain, the spatiotemporal trend of the original satellite AOD data is removed using the spatiotemporal moving window filter method (Lee et al., 2008). The spatiotemporal trend component AOD(x, y, t) was calculated using the mean value of AODs at pixels within the filter window (x ± 20 grids, y ± 20 grids, and t ± 2 days) that were extracted from the original data. The residuals were assumed to be spatiotemporally stationary and were used for the spatiotemporal covariance calculation (Fig. 3).

In spatiotemporal geo-statistics, the spatiotemporal covariance is a function of distance in space and time (Fig. 3). Covariance functions are used to present the spatiotemporal dependency of the known data field and then to estimate the entire random field. We modeled the spatiotemporal covariance of the detrended AOD field by using a nested spatiotemporal covariance model with a sum of two combined models (exponential/spherical and spherical/exponential):

$$C(r,\tau) = C_1 exp\left(-\frac{r}{a_{r1}}\right)\left[1 - \frac{3\tau}{2a_{\tau1}} + \frac{\tau^3}{2a_{\tau1}^3}\right] + C_2\left[1 - \frac{3r}{2a_{r2}} + \frac{r^3}{2a_{r2}^3}\right] exp\left(-\frac{\tau}{a_{\tau2}}\right) \quad (10)$$

Where r is the spatial lag and τ is the temporal lag between AOD grids at coordinates (x, y, t) and coordinates (x′, y′, t′). C1 and C2 are the partial sill variances of the two models. a_{r1} and a_{r2} are the spatial ranges of the two combined models; $a_{\tau1}$ and $a_{\tau2}$ are the temporal ranges of the two models (Hayunga and Kolovos, 2016).

For comparison, two BME AOD products are derived, i.e., BME-S AOD derived with only soft data and BME-SH AOD derived with satellite and sunphotometer AOD as soft and hard data, respectively. Since hard data exert little influence on the covariance model, the parameters of the BME-S AOD covariance model in Table 1 are also used for the BME-SH AOD production. The coefficient of determination parameter (R^2), the mean prediction error (MPE), and the root mean squared error (RMSE) are used to evaluate the performance.

3. Results

Since seasonal $PM_{2.5}$ values if the presence of satellite AOD retrievals are notably lower than the counterparts in the absence of AOD in the autumn and winter (Song et al., 2019), we quantitatively assessed the extent to which the BME improved MODIS AOD coverage and thereby $PM_{2.5}$ estimation in these two seasons.

3.1. BME-based AOD data fusion

Fig. 4 presents the statistics of original MODIS, BME-S and BME-SH AOD. The averaged completeness of the original MODIS data over NCP is 52.4%. The BME substantially improves the AOD completeness. The BME-S AOD and BME-SH AOD, with seasonal averaged completeness of 94.8% and 95.7%, respectively. The spatial mean and standard deviation values of MODIS AOD and COV (coefficient of variation, ratio of one standard deviation to mean in temporal scale) over NCP are 0.42±0.25 and 103.5%±37.5%. Larger COV of AOD indicates larger temporal AOD variability and therefore to some extent indicating larger $PM_{2.5}$ variability. With the application of the BME method, the seasonal mean BME-S AOD value is 0.48±0.28 and AOD is 0.49±0.27 for the BME-SH method. The BME leads to a notably increase in mean AOD and its standard deviation, which is consistent with our expectation that heavy aerosol pollution events are often misclassified into cloud by the MODIS cloud screening algorithm. This is very likely leading to potentially lower AOD and then $PM_{2.5}$.

The quality of the BME merged AOD product is assessed by comparing independent AERONET data at Beijing-RADI (Fig. 5). Daily AOD from sun-photometer is matched with the average of AOD retrievals within 30 km of the station. The original MODIS product is in good agreement with AERONET AOD, which is characterized by R^2 of 0.84, MPE of 0.11 and RMSE of 0.16. The quality of the BME-S AOD product is slightly worse than the original AOD, which is reflected by R^2 of 0.70, MPE of 0.16 and RMSE (0.29). This is likely because the BME method is based on the spatiotemporal trend and covariance of data, which certainly smooths the spatiotemporal variation to some extent. Combining surface-based AOD measurements, the quality of BME-SH AOD is comparable to that of the original MODIS data (R^2 of 0.85, MPE of 0.10 and RMSE of 0.22). Therefore, it would be encouraging by incorporating not only soft data but also hard data into the BME method because the latter is able to produce the merged AOD data with not only good completeness but also high quality.

3.2. LME model validation

CV results of $PM_{2.5}$ concentrations based on three different AOD datasets are presented in Fig. 6. Three quantitative parameters of CV based on 24350 collocated daily MODIS AOD and $PM_{2.5}$ data points, i.e., R^2, MPE, and RMSE are 0.76, 18.7 μg m^{-3} and 29.0 μg m^{-3}, respectively. This CV performance is similar to the work of Zheng et al. (2016), which evaluated LME model in Beijing−Tianjin−Hebei area with an R^2 = 0.77 and RMSE = 23.1 μg m^{-3}. Compared to the CV results of satellite derived $PM_{2.5}$ from the original MODIS AOD, much more matched data records are available for the BME-S $PM_{2.5}$ estimates (N of 45050, increased by nearly 85%) but show slightly lower accuracy (R^2 of 0.70, MPE of 21.9 μg m^{-3} and RMSE of 36.7 μg m^{-3}). In addition to a remarkable improvement in matched data points, the BME-SH $PM_{2.5}$ CV validation shows a comparable accuracy to that from the original MODIS AOD, with MPE of 22.2 and RMSE of 33.8 μg m^{-3}. As expected, the BME resulted in much larger AOD and thereby $PM_{2.5}$, for

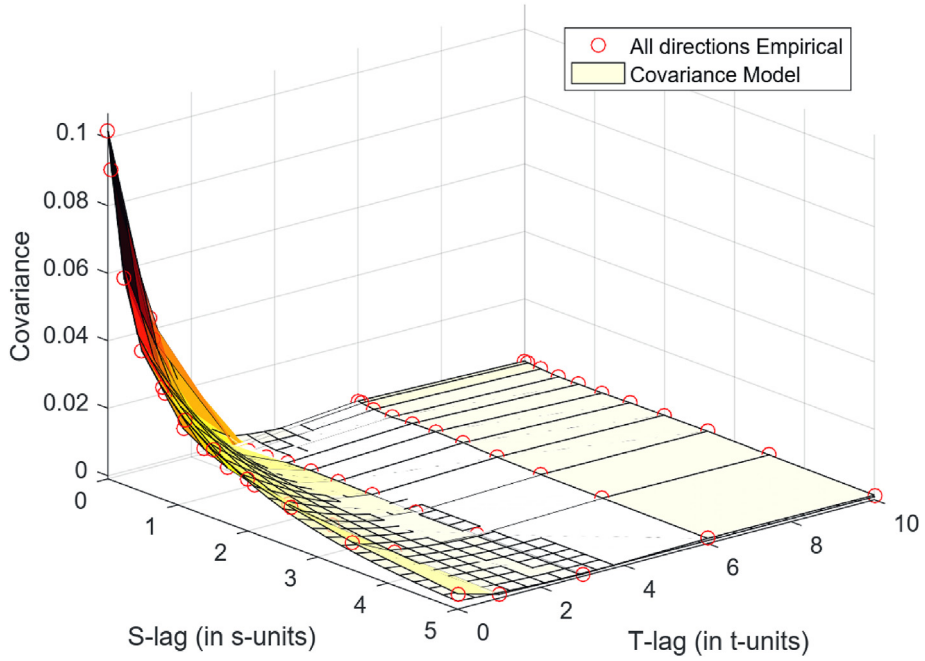

Fig. 3. Calculated and the modeled spatiotemporal covariance (based on the residuals from soft data).

Table 1
Parameters of the fitted spatiotemporal covariance models.

	MODEL-TYPE	Sill	Part1(a_{r1}, a_{r2})	Part2($a_{\tau 1}$, $a_{\tau 2}$)
BME-S	exponential/spherical	0.0621	4.0000	3.0000
	spherical/exponential	0.0400	0.4000	3.0000

example, the percentage of $PM_{2.5}$ exceeding 100 μg m^{-3} increased by 2.7%. A previous study by Lv et al. (2016) used a novel two-step method (linear regression and ordinary Kriging methods) to predict missing AOD values, with R^2 = 0.78 for $PM_{2.5}$ in the 10-fold leave-10%-monitors-out cross validation. In this study, the value of R^2 (0.74) in CV is comparable to previous one, meanwhile, AOD products have high accuracy (R^2 of 0.85 in Fig. 5).

3.3. $PM_{2.5}$ estimation and evaluation

Spatial distributions of seasonal mean $PM_{2.5}$ concentrations derived from three AOD datasets are shown in Fig. 7, in which station mean $PM_{2.5}$ values are overlaid for comparison. Averaged $PM_{2.5}$ concentrations over NCP were 70.1±12.1, 74.0±11.8 and 75.8±10.7 μg m^{-3} derived from these three datasets, respectively. Increase in seasonal $PM_{2.5}$ based on BME AOD is associated with much more AOD-$PM_{2.5}$ pairs with high $PM_{2.5}$ values. $PM_{2.5}$ values in the central part of NCP (Hebei and Shandong Province) estimated from the BME AOD (S or SH) are larger than those from MODIS AOD by > 10 μg m^{-3}, which is much closer to the ground truth. Considering the sampling rate over this region in Fig. 4, AOD filling using BME method over polluted areas can substantially improve $PM_{2.5}$ estimation.

Fig. 8 depicts time series of daily mean differences between retrieved and measured $PM_{2.5}$ concentrations over entire ground $PM_{2.5}$ sites. $PM_{2.5}$ concentrations derived from the original MODIS AOD usually tend to produce abnormal deviation from ground measurements. For example, MODIS AOD retrieved $PM_{2.5}$ biased from ground measurements by 84.0 and 112.1 μg m^{-3} on 21 November, 2014 and 06 January, 2015, respectively. This is in accordance with the expectation that MODIS AOD cannot capture heavy pollution and cloudy days. Fig. 9 shows a case study searching potential error sources of these large $PM_{2.5}$ biases. In this four-day case, almost the entire NCP was covered by clouds or haze. On 20 October, 2014, valid MODIS retrieved AODs were sparsely scattered in northwest of NCP and AOD values were relatively low in this area. Large underestimation (−55.0 μg m^{-3}) is not surprising if only based on these limited AODs to derived $PM_{2.5}$ concentrations. Two contrary cases occurred on 30 October, 2014 and 01 November, 2014 when very high MODIS AODs were found in a few pixels. In consequence, $PM_{2.5}$ estimated from these pixels would have produced positive biases against ground truth. By applying the BME method to MODIS AOD products, the daily mean difference of $PM_{2.5}$ has decreased to 7.7 μg m^{-3} and most of abnormal differences are eliminated. More accurate retrievals are from the BME-SH AOD as the difference reduces to 6.9 μg m^{-3}. In total, BME-SH AOD derived $PM_{2.5}$ can well reproduce the temporal short-term variation of $PM_{2.5}$ across the NCP, which would favor for daily exposure assessment.

Improvement of seasonal $PM_{2.5}$ estimation as a result of AOD sampling enhancement by the BME is clearly shown in Fig. 10, in which seasonal mean $PM_{2.5}$ values at 264 stations derived from AOD are compared with surface measurements. As shown in the left panel, retrieved seasonal $PM_{2.5}$ from the original MODIS AOD has a remarkable underestimation when surface concentration exceeds 100 μg m^{-3}. Stations with high $PM_{2.5}$ concentrations (> 100 μg m^{-3}) almost share the feature that sampling rate is less than 50%. After filling the missing MODIS AOD value, BME-S AOD has much better performance in the derivation of seasonal mean $PM_{2.5}$ by increased R^2 (0.96), decreased MPE (3.7 μg m^{-3}) and RMSE (5.8 μg m^{-3}). Further improvement is evidenced if hard data are included in the BME method, with MPE and RMSE decreasing to 3.5 and 5.5 μg m^{-3}, respectively. Underestimation of $PM_{2.5}$ at heavy pollution stations is substantially overcome.

4. Conclusions and discussion

In order to improve MODIS AOD coverage in NCP where non-random AOD missing is not rare, a few procedures have been adopted. We created the linear relationship between Terra AOD and Aqua AOD to obtain a more complete daily mean AOD. BME was implemented for combining satellite AOD and sunphotometer AOD to produce AOD fields with good spatiotemporal coverage and high quality. Potential contribution of filling AOD gaps by using the BME to the $PM_{2.5}$ prediction has been investigated. Major conclusions are as follows.

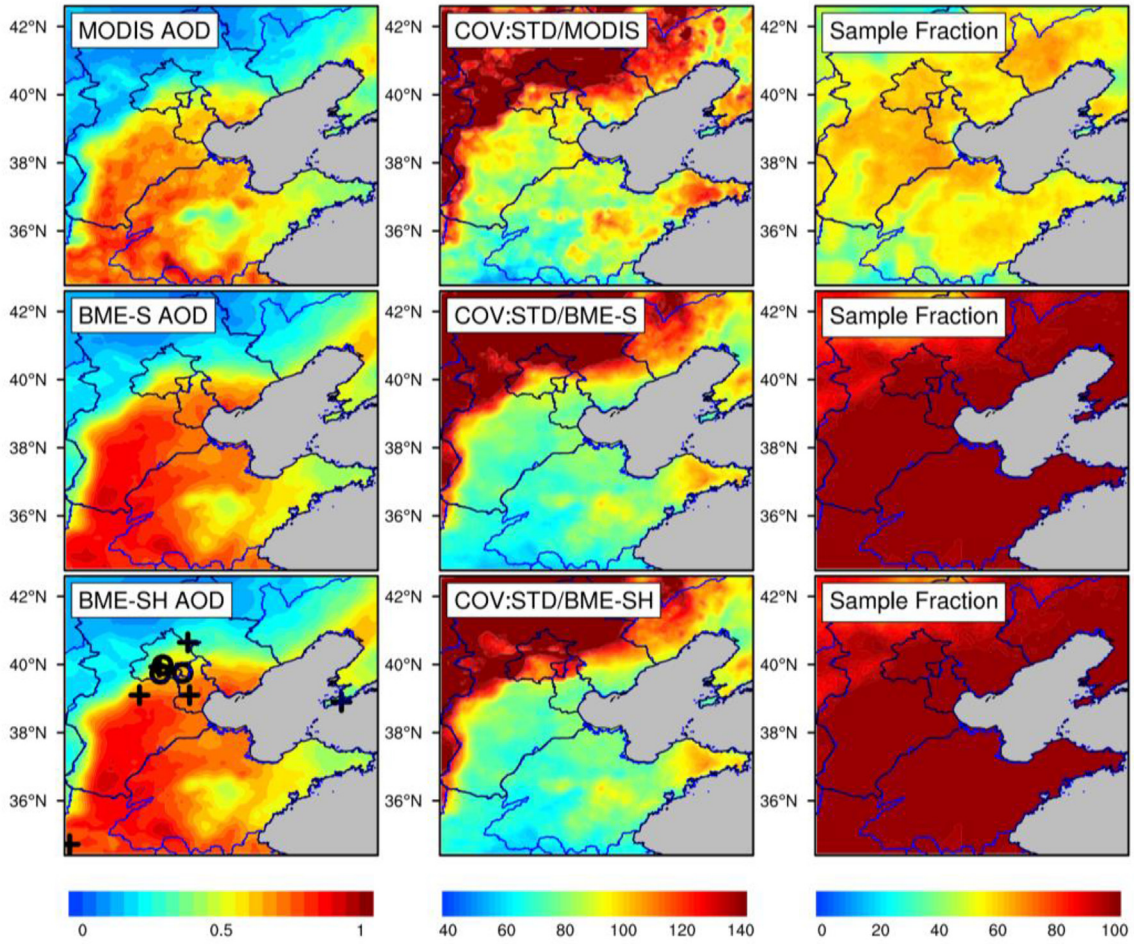

Fig. 4. Sample fraction of MODIS AOD, BME-S AOD and BME-SH data. Three columns are seasonal mean AOD, coefficient of variation (COV) for AOD (ratio of one standard deviation to mean) and the sampling rate (fraction of days with AOD retrievals to total days) from left to right. Three rows represent the results for MODIS AOD, BME-S AOD and BME-SH AOD, respectively.

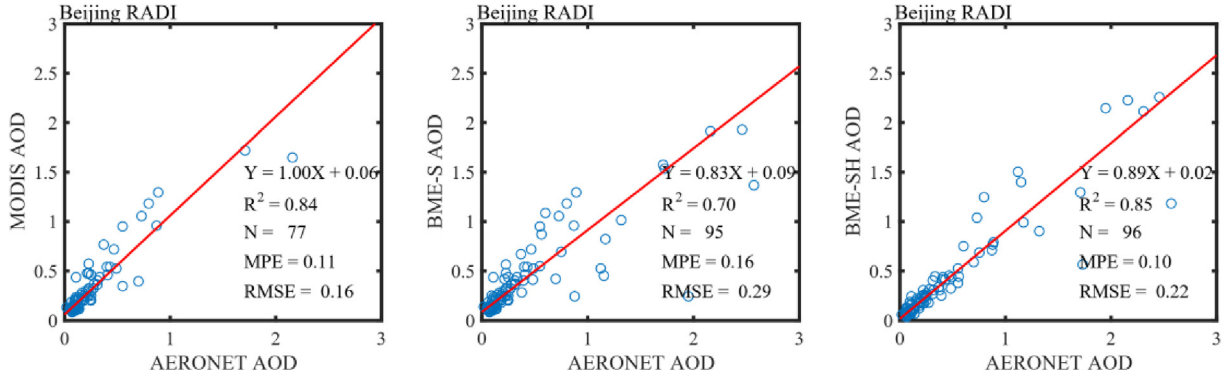

Fig. 5. Comparisons of AERONET Beijing-RADI AOD against MODIS AOD, BME-S AOD and BME-SH AOD in cold season of 2014.

By applying the BME method to MODIS AOD, a spatiotemporally coherent daily AOD dataset was produced over NCP. The seasonal mean completeness of the BME-S AOD is 94.8%, which is much higher than that of MODIS AOD data (52.4%). The comparison of BME-S AOD against AERONET RADI site shows a systematic underestimation (R^2 of 0.70, slope of 0.83). A more accurate AOD product (with R^2 of 0.85, slope of 0.89) can be derived when the AERONET/CARSNET data are synergized into the model. Monthly $PM_{2.5}$ predictions from the original MODIS AOD are generally smaller than corresponding ground measurements, especially in these polluted stations. Daily variation of and monthly mean $PM_{2.5}$ concentrations are substantially improved from the BME derived AOD fields with enhancement of AOD spatiotemporal completeness.

As a robust probabilistic method, BME can substantially increase MODIS AOD sampling. Moreover, the accuracy of the BME-derived AOD products can be remarkably improved if sun-photometer AOD data are incorporated in the model. It should be noted that current sunphotometer stations are mostly located in north of NCP. . Further deployment of AERONET/CARSNET sites in south of NCP may further improve the performance of the BME method (Li et al., 2015) given the fact that the spatial representativeness of sunphotomter station is limited (Fu et al., 2018).

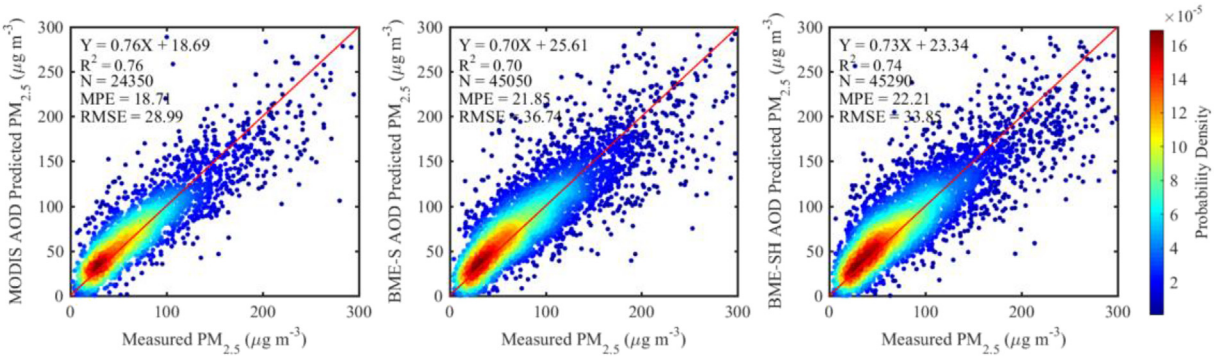

Fig. 6. Cross validation of daily $PM_{2.5}$ estimation from MODIS AOD (left), BME-S AOD (middle) and BME-SH AOD (right).

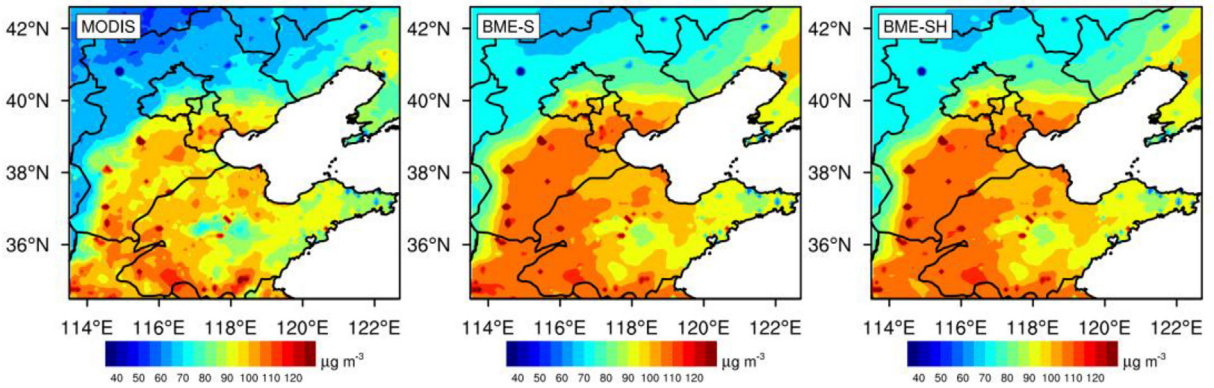

Fig. 7. $PM_{2.5}$ concentration maps retrieved using only MODIS AOD (left), BME-S AOD (middle) and BME-SH AOD data (right).

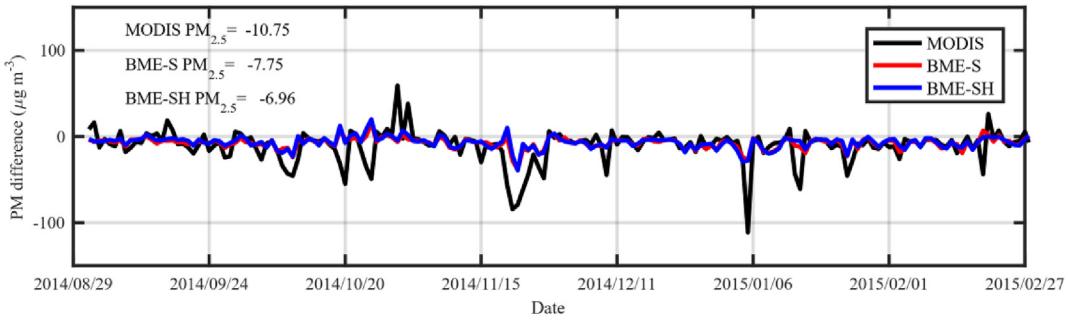

Fig. 8. The differences between ground site measurements and retrieved $PM_{2.5}$ concentrations based on original MODIS AOD (black), BME-S (red) and BME-SH (blue) AOD products.

The performance of this fusion method depends on the data availability. In areas where MODIS AODs have large data gaps in space and time, insufficient observations may lead to physically unrealistic features in the merged AOD data. Considering more satellite AOD products with different retrieval protocols as soft data for the BME may improve the BME performance in filling AOD gaps. We used MODIS 10 km AOD data that may not capture fine features of local aerosol pollution, which may be remedied by using satellite AOD products with finer resolution, for example, the Multi-Angle Implementation of Atmospheric Correction (MAIAC) aerosol products with resolution of 1 km (Lyapustin et al., 2011).

Previous studies used a few statistical methods to fill AOD gaps, for example, the random forest method (Zhang et al., 2018). This method requires many other geographical variables, for example, land use and meteorological variables. Though the random forest method is less sensitive to overfitting than other machine learning methods (Belgiu and Drăgu, 2016), this issue is not completely fixed yet since so many variables are incorporated. On the contrary, the BME only requires AOD as input that facilitates its application. Since results on the AOD filling are based on different methods in different regions, we appeal for a carefully organized study to evaluate the performances of all these data filling methods that should be performed under the same condition.

Author contributions

Disong Fu: Conceived and designed the analysis, Collected the data, Contributed data or analysis tools, Performed the analysis, Wrote the paper, Other contribution Reply reviewers. **Zijue Song**: Collected the data, Performed the analysis, Wrote the paper. **Xiaoling Zhang**: Conceived and designed the analysis, Wrote the paper Revise the paper. **Xiangao Xia**: Conceived and designed the analysis, Wrote the paper Revise the paper, Other contribution Providing funds and replying the reviewers. **Jun Wang**: Conceived and designed the analysis, Wrote the paper Providing suggestions for context and coverletter, Other contribution Fund. **Huizheng Che**: Collected the data CARSNET data, Other contribution Suggestions of organization of manuscript.

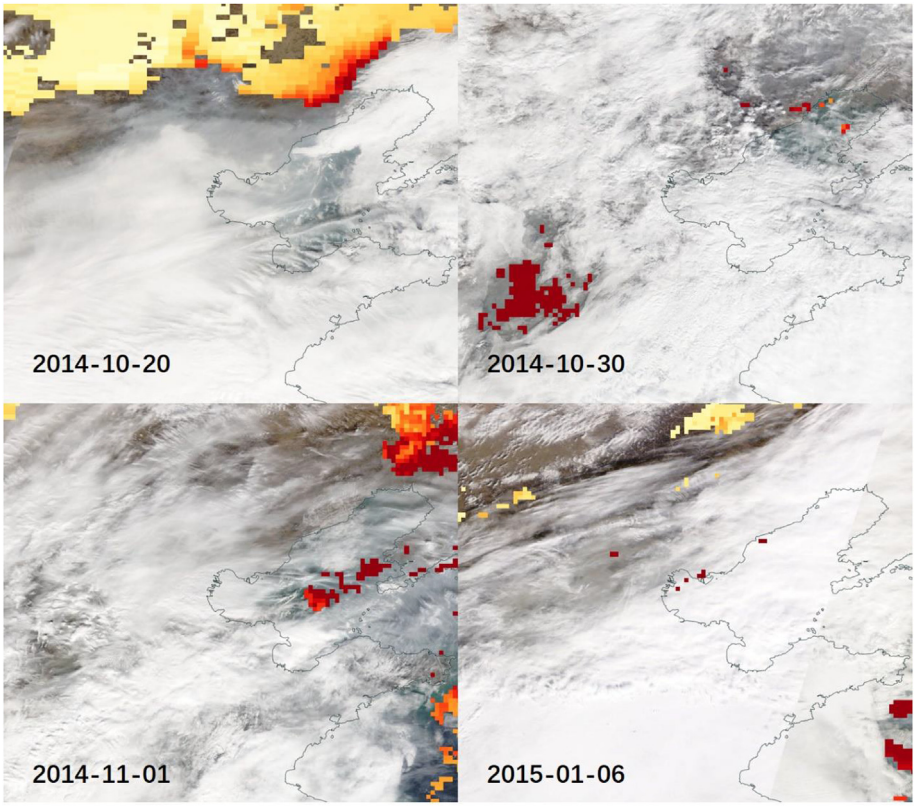

Fig. 9. MODIS RGB images in North China Plain overlaid with daily MODIS AOD retrievals.

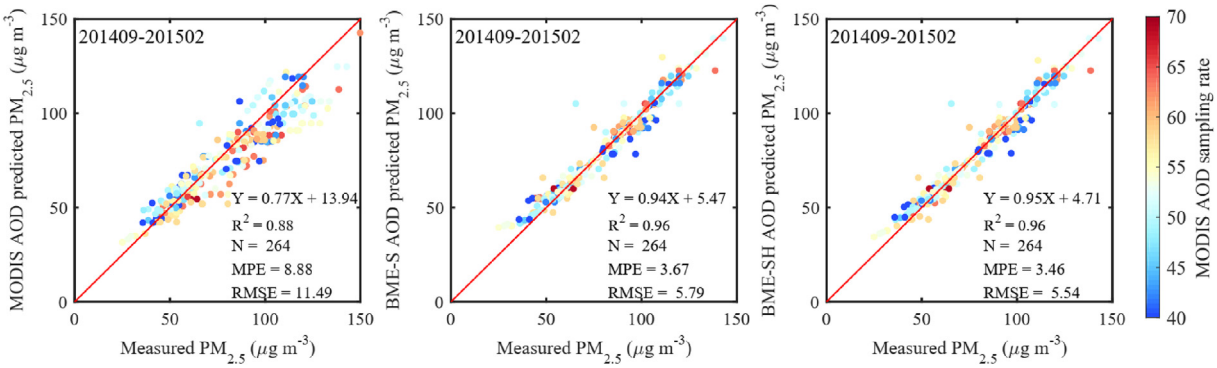

Fig. 10. Scatter plots of the MODIS (left), BME-S (middle) and BME-SH AOD (right) derived seasonal mean $PM_{2.5}$ against ground-observed $PM_{2.5}$ at 264 ground sites during September 2014 to February 2015. The colorbar represents the MODIS AOD sampling rates at each station.

Huangjian Wu: Collected the data PM2.5 hourly data, Contributed data or analysis tools Quality control of PM2.5 data. **Xiao Tang**: Collected the data PM2.5 data. Contributed data or analysis tools Quality control of PM2.5 data. **Jinqiang Zhang**: Other contribution Fund. **Minzheng Duan**: Conceived and designed the analysis.

Declaration of competing interest

We confirm that the manuscript approved by all named authors and declare that we have no financial and personal relationships with other people or organizations that can inappropriately influence our work. The authors declared that they have no conflicts of interest to this work.

Acknowledgements

This work is supported by the National Science Foundation of China (91644217, 41475138), the National Key Research and Development Program of China (2016YFC0200403, 2017YFA0603504). J. Wang is supported by the faculty startup funds in the University of Iowa.

References

Belgiu, M., Drăgu, L., 2016. Random forest in remote sensing: a review of applications and future directions. ISPRS J. Photogrammetry Remote Sens. 114, 24–31. https://doi.org/10.1016/j.isprsjprs.2016.01.011.

Che, H., Xia, X., Zhu, J., Li, Z., Dubovik, O., Holben, B., Goloub, P., Chen, H., Estelles, V., Cuevas-Agulló, E., Blarel, L., Wang, H., Zhao, H., Zhang, X., Wang, Y., Sun, J., Tao, R., Zhang, X., Shi, G., 2014. Column aerosol optical properties and aerosol radiative forcing during a serious haze-fog month over North China Plain in 2013 based on ground-based sunphotometer measurements. Atmos. Chem. Phys. 14, 2125–2138. https://doi.org/10.5194/acp-14-2125-2014.

Christakos, G., 1990a. A Bayesian/maximum-entropy view to the spatial estimation problem. Math. Geol. 22, 763–777. https://doi.org/10.1007/BF00890661.

Christakos, G., 1990b. Modern Spatiotemporal Geostatistics. OXFORD UNIVERSITY PRESS.

Christakos, G., Serre, M.L., 2000. BME analysis of spatiotemporal particulate matter distributions in North Carolina. Atmos. Environ. 34, 3393–3406. https://doi.org/10.1016/S1352-2310(00)00080-7.

Chudnovsky, A., Tang, C., Lyapustin, A., Wang, Y., Schwartz, J., Koutrakis, P., 2013. A critical assessment of high-resolution aerosol optical depth retrievals for fine particulate matter predictions. Atmos. Chem. Phys. 13, 10907–10917. https://doi.org/10.5194/acp-13-10907-2013.

Eck, T.F., Holben, B.N., Reid, J.S., Dubovik, O., Smirnov, A., O'Neill, N.T., Slutsker, I., Kinne, S., 1999. Wavelength dependence of the optical depth of biomass burning, urban, and desert dust aerosols. J. Geophys. Res. Atmos. 104, 31333–31349. https://doi.org/10.1029/1999JD900923.

Eck, T.F., Holben, B.N., Reid, J.S., Xian, P., Giles, D.M., Sinyuk, A., Smirnov, A., Schafer, J.S., Slutsker, I., Kim, J., Koo, J.H., Choi, M., Kim, K.C., Sano, I., Arola, A., Sayer, A.M., Levy, R.C., Munchak, L.A., O'Neill, N.T., Lyapustin, A., Hsu, N.C., Randles, C.A., Da Silva, A.M., Buchard, V., Govindaraju, R.C., Hyer, E., Crawford, J.H., Wang, P., Xia, X., 2018. Observations of the interaction and transport of fine mode aerosols with cloud and/or fog in northeast asia from aerosol robotic network and satellite remote sensing. J. Geophys. Res. Atmos. 123, 5560–5587. https://doi.org/10.1029/2018JD028313.

Fu, D., Xia, X., Wang, J., Zhang, X., Li, X., Liu, J., 2018. Synergy of AERONET and MODIS AOD products in the estimation of $PM_{2.5}$ concentrations in Beijing. Sci. Rep. 8, 2–9. https://doi.org/10.1038/s41598-018-28535-2.

Geng, G., Zhang, Q., Martin, R.V., Donkelaar, A., Van, Huo, H., Che, H., Lin, J., He, K., 2015. Remote Sensing of Environment Estimating long-term $PM_{2.5}$ concentrations in China using satellite-based aerosol optical depth and a chemical transport model. Remote Sens. Environ. 166, 262–270. https://doi.org/10.1016/j.rse.2015.05.016.

Gupta, P., Levy, R.C., Mattoo, S., Remer, L.A., Munchak, L.A., 2016. A surface reflectance scheme for retrieving aerosol optical depth over urban surfaces in MODIS Dark Target retrieval algorithm. Atmos. Meas. Tech. 9, 3293–3308. https://doi.org/10.5194/amt-9-3293-2016.

Gupta, P., Remer, L.A., Levy, R.C., Mattoo, S., 2018. Validation of MODIS 3km land aerosol optical depth from NASA's EOS Terra and Aqua missions. Atmos. Meas. Tech. 11, 3145–3159. https://doi.org/10.5194/amt-11-3145-2018.

Hayunga, D.K., Kolovos, A., 2016. Geostatistical space–time mapping of house prices using Bayesian maximum entropy. Int. J. Geogr. Inf. Sci. 30, 2339–2354. https://doi.org/10.1080/13658816.2016.1165820.

He, J., Christakos, G., 2018. Space-time $PM_{2.5}$ mapping in the severe haze region of Jing-Jin-Ji (China) using a synthetic approach. Environ. Pollut. 240, 319–329. https://doi.org/10.1016/j.envpol.2018.04.092.

Hoek, G., Krishnan, R.M., Beelen, R., Peters, A., Ostro, B., Brunekreef, B., Kaufman, J.D., 2013. Long-term air pollution exposure and cardio- respiratory mortality: a review. Environ. Health 12, 43. https://doi.org/10.1186/1476-069X-12-43.

Holben, B.N., Eck, T.F., Slutsker, I., Tanré, D., Buis, J.P., Setzer, A., Vermote, E., Reagan, J.A., Kaufman, Y.J., Nakajima, T., Lavenu, F., Jankowiak, I., Smirnov, A., 1998. AERONET—a federated instrument network and data archive for aerosol characterization. Remote Sens. Environ. 66, 1–16. https://doi.org/10.1016/S0034-4257(98)00031-5.

Hsu, N.C., Jeong, M.J., Bettenhausen, C., Sayer, A.M., Hansell, R., Seftor, C.S., Huang, J., Tsay, S.C., 2013. Enhanced Deep Blue aerosol retrieval algorithm: the second generation. J. Geophys. Res. Atmos. 118, 9296–9315. https://doi.org/10.1002/jgrd.50712.

Lee, H.J., Liu, Y., Coull, B.A., Schwartz, J., Koutrakis, P., 2011. A novel calibration approach of MODIS AOD data to predict $PM_{2.5}$ concentrations. Atmos. Chem. Phys. 11, 7991–8002. https://doi.org/10.5194/acp-11-7991-2011.

Lee, S.J., Balling, R., Gober, P., 2008. Bayesian maximum entropy mapping and the soft data problem in urban climate research. Ann. Assoc. Am. Geogr. 98, 309–322. https://doi.org/10.1080/00045600701851184.

Levy, R.C., Mattoo, S., Munchak, L.A., Remer, L.A., Sayer, A.M., Patadia, F., Hsu, N.C., 2013. The Collection 6 MODIS aerosol products over land and ocean. Atmos. Meas. Tech. 6, 2989–3034. https://doi.org/10.5194/amt-6-2989-2013.

Li, J., Carlson, B.E., Lacis, A.A., 2015. How well do satellite AOD observations represent the spatial and temporal variability of $PM_{2.5}$ concentration for the United States? Atmos. Environ. 102, 260–273.

Liu, Y., Sarnat, J.A., Kilaru, V., Jacob, D.J., Koutrakis, P., 2005. Estimating ground-level $PM_{2.5}$ in the eastern United States using satellite remote sensing. Environ. Sci. Technol. 39, 3269–3278. https://doi.org/10.1021/es049352m.

Lv, B., Hu, Y., Chang, H.H., Russell, A.G., Bai, Y., 2016. Improving the accuracy of daily $PM_{2.5}$ distributions derived from the fusion of ground-level measurements with aerosol optical depth observations, a case study in north China. Environ. Sci. Technol. 50, 4752–4759. https://doi.org/10.1021/acs.est.5b05940.

Lv, B., Hu, Y., Chang, H.H., Russell, A.G., Cai, J., Xu, B., Bai, Y., 2017. Daily estimation of ground-level $PM_{2.5}$ concentrations at 4 km resolution over Beijing-Tianjin-Hebei by fusing MODIS AOD and ground observations. Sci. Total Environ. 580, 235–244. https://doi.org/10.1016/j.scitotenv.2016.12.049.

Lyapustin, A., Wang, Y., Laszlo, I., Kahn, R., Korkin, S., Remer, L., Levy, R., Reid, J.S., 2011. Multiangle implementation of atmospheric correction (MAIAC): 2. Aerosol algorithm. J. Geophys. Res. Atmos. 116, 1–15.

Ma, Z., Hu, X., Huang, L., Bi, J., Liu, Y., 2014. Estimating ground-level $PM_{2.5}$ in China using satellite remote sensing. Environ. Sci. Technol. 48, 7436–7444. https://doi.org/10.1021/es5009399.

Modis, K., Vatalis, K.I., Sachanidis, C., 2013. Spatiotemporal risk assessment of soil pollution in a lignite mining region using a Bayesian maximum entropy (BME) approach. Int. J. Coal Geol. 112, 173–179.

Pope, C.A., Dockery, D.W., 2006. Health effects of fine particulate air pollution: lines that connect. J. Air Waste Manag. Assoc. 56, 709–742. https://doi.org/10.1080/10473289.2006.10464485.

Pope III, C.A., 2002. Lung cancer, cardiopulmonary mortality, and long-term exposure to fine particulate air pollution. J. Am. Med. Assoc. 287, 1132. https://doi.org/10.1001/jama.287.9.1132.

Pui, D.Y.H., Chen, S.-C., Zuo, Z., 2014. $PM_{2.5}$ in China: measurements, sources, visibility and health effects, and mitigation. Particuology 13, 1–26. https://doi.org/10.1016/j.partic.2013.11.001.

Qu, W., Wang, J., Zhang, X., Sheng, L., Wang, W., 2016. Opposite Seasonality of the Aerosol Optical Depth and the Surface Particulate Matter Concentration over the North China Plain. Atmospheric Environment. Elsevier Ltdhttps://doi.org/10.1016/j.atmosenv.2015.11.061.

Shi, T., Yang, X., Christakos, G., Wang, J., Liu, L., 2015. Spatiotemporal interpolation of rainfall by combining BME theory and satellite rainfall estimates. Atmosphere 6, 1307–1326. https://doi.org/10.3390/atmos6091307.

Song, Z., Fu, D., Zhang, X., Han, X., Song, J., Zhang, J., Wang, J., Xia, X., 2019. MODIS AOD sampling rate and its potential effect on seasonal $PM_{2.5}$ estimation in North China. Atmos. Environ 209, 14–22. https://doi.org/10.1016/j.atmosenv.2019.04.020.

Song, Z., Fu, D., Zhang, X., Wu, Y., Xia, X., He, J., Han, X., Zhang, R., Che, H., 2018. Diurnal and seasonal variability of $PM_{2.5}$ and AOD in North China plain: comparison of MERRA-2 products and ground measurements. Atmos. Environ. 191, 70–78. https://doi.org/10.1016/j.atmosenv.2018.08.012.

Strickland, M.J., Hao, H., Hu, X., Chang, H.H., Darrow, L.A., Liu, Y., 2016. Pediatric emergency visits and short-term changes in $PM_{2.5}$ concentrations in the U.S. State of Georgia. Environ. Health Perspect. 124, 690–696. https://doi.org/10.1289/ehp.1509856.

Tang, Q., Bo, Y., Zhu, Y., 2016. Spatiotemporal fusion of multiple-satellite aerosol optical depth (AOD) products using Bayesian maximum entropy method. J. Geophys. Res. Atmos. 121, 4034–4048. https://doi.org/10.1002/2015JD024571.

Van Donkelaar, A., Martin, R.V., Brauer, M., Boys, B.L., 2015. Use of satellite observations for long-term exposure assessment of global concentrations of fine particulate matter. Environ. Health Perspect. 123, 135–143. https://doi.org/10.1289/ehp.1408646.

Van Donkelaar, A., Martin, R.V., Brauer, M., Hsu, N.C., Kahn, R.A., Levy, R.C., Lyapustin, A., Sayer, A.M., Winker, D.M., 2016. Global estimates of fine particulate matter using a combined geophysical-statistical method with information from satellites, models, and monitors. Environ. Sci. Technol. 50, 3762–3772. https://doi.org/10.1021/acs.est.5b05833.

Van Donkelaar, A., Martin, R.V., Levy, R.C., da Silva, A.M., Krzyzanowski, M., Chubarova, N.E., Semutnikova, E., Cohen, A.J., 2011. Satellite-based estimates of ground-level fine particulate matter during extreme events: a case study of the Moscow fires in 2010. Atmos. Environ. 45, 6225–6232. https://doi.org/10.1016/j.atmosenv.2011.07.068.

Wang, J., Christopher, S.A., 2003. Intercomparison between satellite-derived aerosol optical thickness and $PM_{2.5}$ mass: implications for air quality studies. Geophys. Res. Lett. 30, 2095. https://doi.org/10.1029/2003GL018174.

Wu, H., Tang, X., Wang, Z., Wu, L., Lu, M., Wei, L., Zhu, J., 2018. Probabilistic automatic outlier detection for surface air quality measurements from the China national environmental monitoring network. Adv. Atmos. Sci. 35, 1522–1532. https://doi.org/10.1007/s00376-018-8067-9.

Wu, J., Yao, F., Li, W., Si, M., 2016. VIIRS-based remote sensing estimation of ground-level $PM_{2.5}$ concentrations in Beijing–Tianjin–Hebei: a spatiotemporal statistical model. Remote Sens. Environ. 184, 316–328. https://doi.org/10.1016/j.rse.2016.07.015.

Xia, X.A., Chen, H.B., Wang, P.C., Zhang, W.X., Goloub, P., Chatenet, B., Eck, T.F., Holben, B.N., 2006. Variation of column-integrated aerosol properties in a Chinese urban region. J. Geophys. Res. Atmos. 111, 1–10. https://doi.org/10.1029/2005JD006203.

Xiao, Q., Wang, Y., Chang, H.H., Meng, X., Geng, G., Lyapustin, A., Liu, Y., 2017. Full-coverage high-resolution daily $PM_{2.5}$ estimation using MAIAC AOD in the Yangtze River Delta of China. Remote Sens. Environ. 199, 437–446. https://doi.org/10.1016/j.rse.2017.07.023.

Yu, H.-L., Kolovos, A., Christakos, G., Chen, J.-C., Warmerdam, S., Dev, B., 2007. Interactive spatiotemporal modelling of health systems: the SEKS–GUI framework. Stoch. Environ. Res. Risk Assess. 21, 555–572. https://doi.org/10.1007/s00477-007-0135-0.

Zhan, Y., Luo, Y., Deng, X., Chen, H., Grieneisen, M.L., Shen, X., Zhu, L., Zhang, M., 2017. Spatiotemporal prediction of continuous daily $PM_{2.5}$ concentrations across China using a spatially explicit machine learning algorithm. Atmos. Environ. 155, 129–139. https://doi.org/10.1016/j.atmosenv.2017.02.023.

Zhang, R., Di, B., Luo, Y., Deng, X., Grieneisen, M.L., Wang, Z., Yao, G., Zhan, Y., 2018. A nonparametric approach to filling gaps in satellite-retrieved aerosol optical depth for estimating ambient $PM_{2.5}$ levels. Environ. Pollut. 243, 998–1007. https://doi.org/10.1016/j.envpol.2018.09.052.

Zheng, Y., Zhang, Q., Liu, Y., Geng, G., He, K., 2016. Estimating ground-level $PM_{2.5}$ concentrations over three megalopolises in China using satellite-derived aerosol optical depth measurements. Atmos. Environ. 124, 232–242. https://doi.org/10.1016/j.atmosenv.2015.06.046.